Volume 18, Number 5, 2025. pp. 629-642

Jordan Journal of Physics

ARTICLE

The Photothermal Conversion Characteristics of a Selective Coating Decorated with ZrO_2 and Fe Powders

Mustafa Ashoor Ryadh and **Ahmed A. Al-Tabbakh**

Department of Physics, College of Science, Al-Nahrain University, Jadiriya, Baghdad, Iraq.

Doi: **https://doi.org/10.47011/18.5.6**

Received on: 10/11/2024; *Accepted on: 23/02/2025*

Abstract: The photothermal conversion characteristics of black, composite, and selective coatings were investigated. ZrO_2 and Fe particles were incorporated into the heat-resistant black paint (HRP) to improve the conversion capability of the coating. The coatings and the particles were applied onto aluminium substrates using the direct spraying method. This resulted in layers having thicknesses of 323.5 μm and 837 μm for the ZrO_2- and Fe-containing coatings. The addition of these powders led to a decrease in the coating density from 1.67 g/cm^3 to 0.31 g/cm^3 and 0.5 g/cm^3 for the ZrO_2/HRP and Fe/HRP coatings, respectively. The addition of the particles was found to improve the solar-to-thermal conversion of the primary paint significantly. Maximum absorbance of 97.81% and a substrate temperature of 382.65 K after 40 minutes of radiation exposure were achieved using the Fe/HRP system. The photothermal conversion characteristics were analyzed based on the structural, compositional, and physical properties of the composite coatings. The absorption spectra in the UV-Vis range of the Fe/HRP coating showed higher peaks than those exhibited by the ZrO_2/HRP coating, emphasizing the higher photo-thermal conversion of the Fe/HRP coating. Owing to their ease of application and high conversion performance, the developed coatings are superior to many existing coating systems for flat-plate collectors.

Keywords: Coating, Photothermal effects, Optical absorption, Nanopowders.

PACS Nos: 42.79. Wc, 78.20. nb, 42.25. Bs, 81.07. Wx.

1. Introduction

Solar-thermal collectors are devices used to capture solar radiation and convert it to heat. They have various designs, structures, and a wide range of applications across industrial and residential sectors. These include space heating, swimming pool and domestic water heating, solar steam generation, and water desalination [1]. Other applications may extend to bacteria killing, catalysis, and sensors. The concentrated and non-concentrated solar collectors for residential and industrial applications depend, in their photothermal conversion and energy harvesting capabilities, on the selective coating on the top of their surfaces [2, 3]. These coatings are responsible for the conversion of solar radiation into thermal energy. The conversion efficiency of the selective coating depends on the coating's structural, elemental, geometrical, and physical characteristics [4-9]. New-generation selective coatings increasingly incorporate nanomaterials and nanostructures in their design to achieve higher absorption coefficients, reduced reflectivity of incident radiation, and enhanced absorption mechanisms such as radiation trapping [8]. In addition, the coatings have to maintain a minimal emittance of energy (i.e., minimal thermal emissivity) at moderate and elevated temperatures. These coatings may be comprised of single or multiple layers of thin or thick films. A large number of materials may also be incorporated for the direct solar conversion application, such as multiwall carbon

Corresponding Author: Ahmed A. Al-Tabbakh **Email**: tabbakh2013@gmail.com

nanotubes (see, for example, Ref. [2]). Atchuta *et al.* produced a thin film of nickel-doped cobaltite spinel on a stainless steel substrate as a selective coating using a wet-chemical dip-coating method [10]. They reported an absorbance of 0.92 of the as-coated substrates. They also succeeded in improving the substrate absorbance to 0.94 by adding an optical enhancement layer on top of the thin film coating. Rubin *et al*. investigated the thermal stability and optical properties of Cu spinel oxide nanoparticles for photothermal conversion [9]. They reported a maximum thermal absorption of 97.2% with high thermal stability of porous Cu-based spinel structures. They investigated the effect of the structural and compositional properties of the coatings on solar absorption. However, no experimental data on the solar-to-thermal conversion were reported in that work.

Sivakumar *et al*. reported a maximum plate-collector temperature of 370 K after coating with a nanofluid composed of black paint mixed with cupric oxide nanoparticles [11]. Mediha *et al*. investigated the effect of doping copper oxide thin films with aluminum on the films' optical and photocatalytic properties [12]. They found that Al-doping affects the crystallite size slightly and improves the electrical conductivity of the thin films. In addition, the energy band gap decreased from 2.62 to 1.8 eV due to the Al-doping. The photocatalysis efficiency of the thin films improved, as shown by the photocatalytic degradation of the orange dye. The photocatalysis mechanism was analyzed based on the generation of electron-hole pairs due to exposure to UV radiation, leading to the production of hydroxyl radicals and reduction of oxygen, which then becomes responsible for dye degradation. The dependence of the photocatalytic effect on temperature and aluminum concentration was also investigated, showing the optimal conditions of these two parameters. The surface morphology of the thin film was found to depend on the aluminum concentration, and this was found to enhance the photocatalytic property of the thin film. This work emphasizes the significant impact of doping with aluminum on the physical and functional properties of copper oxide thin films.

Dikra *et al*. synthesized Zr-doped ZnO thin films for photocatalysis application [13]. They investigated the difference in depositing these films on glass or ceramic substrates, especially on the photocatalytic properties. They found that depositing Zr-doped ZnO films on a ceramic substrate leads to a prominent enhancement of the photocatalytic functionality of the thin films compared with the glass substrate. This was attributed to the effect of the substrate on the structural and electronic properties of the thin films. The substrate seemed to affect the surface roughness of a thin film, the crystallite size, and the material's electronic properties. A notable decrease in the energy band gap was reported to affect the optical and photocatalytic properties of the deposited films. The photocatalytic mechanism was discussed and analyzed based on the electron/hole production and enhanced trapping of the resulting hydroxyl ions on the surface. This work demonstrates that a clear correlation between materials engineering and their functional properties is crucial to developing thin films for different applications. Luka and Ivan reviewed different types of mid- and high-temperature absorber coatings and their fabrication methods [2]. They investigated coatings based on their solar absorptance, thermal emittance, and thermal stability. They showed that spectral selectivity of the coatings is essential for low- and mid-temperature ranges, while highly solar absorption coatings are preferred over their selective counterparts. They also demonstrated the significance of the coating fabrication to be industrially feasible.

The present work aims to investigate the photothermal conversion of a selective coating and the effect of primarily two different particles, these are ZrO_2 and Fe particles, on the solar-thermal conversion parameters. The primary paint, the heat-resistant paint (HRP), was selected due to its pigment type (manganese ferrite), its thermal stability, adhesion characteristics, and availability. Manganese ferrite is known to exhibit excellent optical properties and high solar radiation absorption. achieving efficiencies over 92% in the UV, visible, and near-infrared ranges [14, 15]. Our previous investigation of the paint showed relatively adequate but not sufficiently high conversion characteristics [16, 17]. Thus, we aimed to improve its photothermal conversion by adding micro- and nano-particles. The sought target was to enhance the absorbance by radiation trapping and multiple reflections. The Fe and ZrO_2 particles were not used as a standalone material as they do not fulfill the required photothermal properties. The other

objective was the augmentation of thermal conductivity of the paint without affecting the conversion characteristics of the primary paint. The work is based on measuring and comparing the photothermal responses after the structural and surface modifications made due to the addition of these powders. A key advantage of the proposed approach lies in the development of composite coatings that are simple to apply while maintaining high photothermal conversion efficiency. The photothermal conversion is analyzed based on the compositional, structural, and morphological features of the coatings.

2. Materials and Methods

I. Preparation of Substrates

The substrates used in the present work were cut out from 2 mm-thick aluminum sheets of moderate purity. The 4 cm × 4 cm substrates were subjected to mechanical cleaning, brushing, and degreasing to remove unwanted contaminants from their surfaces. The substrates were washed with detergents, rinsed thoroughly with deionized water, and soaked in acetone to remove grease and other contaminants. The final step of cleaning was air drying. The cleanliness of the surface and its effect on various parameters, such as adhesion of paint and other functional characteristics, is beyond the scope of the present work [18-20]. However, the cleaning procedure adopted presently is believed to maintain the minimum requirements for the successive work and measurements. It is also practically feasible and cost-effective when applied to large surfaces.

II. Application of Primary Paint

Prior to the application of coatings, the substrates were placed in the furnace to ensure their dryness. A heat-resistant black paint from Rust-Oleum Corporation (USA) was used as a primary coating layer. This paint has been utilized in similar research and proved to be compatible with a wide range of additives, allowing for their homogeneous distribution. It is also operable in low to moderate temperatures and has anti-crack characteristics, as will be shown later in this presentation [16, 17]. Table 1 exhibits some of the paint specifications. The substrates were photographed by an ordinary camera before and after being coated, as shown in Figs. 1(a)-(d).

TABLE 1. Specifications of the heat-resistant paint from Rust-Oleum (USA).

Property	Description	
Resin type	V2176838 - Silicone modified alkyd	
Pigment type	Black manganese ferrite	
Solvent	Acetone, Xylene, Toluene, and liquid petroleum gas propellant.	
Dry time at 10-32 °C and 65% relative humidity	1-2 hours	
Relative density with respect to water	0.821	
Dry heat resistance	538 °C	
Composition (%wt.)	Toluene	21 %
	Propane	17 %
	Acetone	14 %
	Black pigment	8.4 %
	Other ingredients	39.6 %

III. The Powders

Two different powders, ZrO_2 and Fe, were added individually to the high-resistant paint. The effect of these additions on solar-to-thermal conversion is compared and discussed in this work. The addition of these powders was performed by an air-spraying process. The powders were initially loaded on the spraying device. After the HRP was applied, the powders were immediately sprayed out from a distance of 30 cm or more while the substrate was slowly rotated to avoid a unidirectional fall of the particles on the substrate surface and maintain a more homogeneous distribution of the powder particles.

IV. Characterization

All the applied coatings were initially inspected visually under an optical microscope. A portable, LED-light source illuminated digital microscope (CoolingTech, 1600× magnification) was used for primary inspection of paint homogeneity. The coating thickness was

measured by means of an LS220 coating thickness gauge (Shenzhen Linshang Technology, China). This gauge provides high-accuracy measurements of coating thickness on ferrous and non-ferrous substrates. The coating thickness was determined by performing several measurements and calculating the average for each substrate. The coatings were also investigated using a scanning electron microscope (Inspect S50 SEM, FEI, Netherlands). This enables inspecting the coating morphology at a microscale or less and investigating the nature of particle integration into the composite coatings.

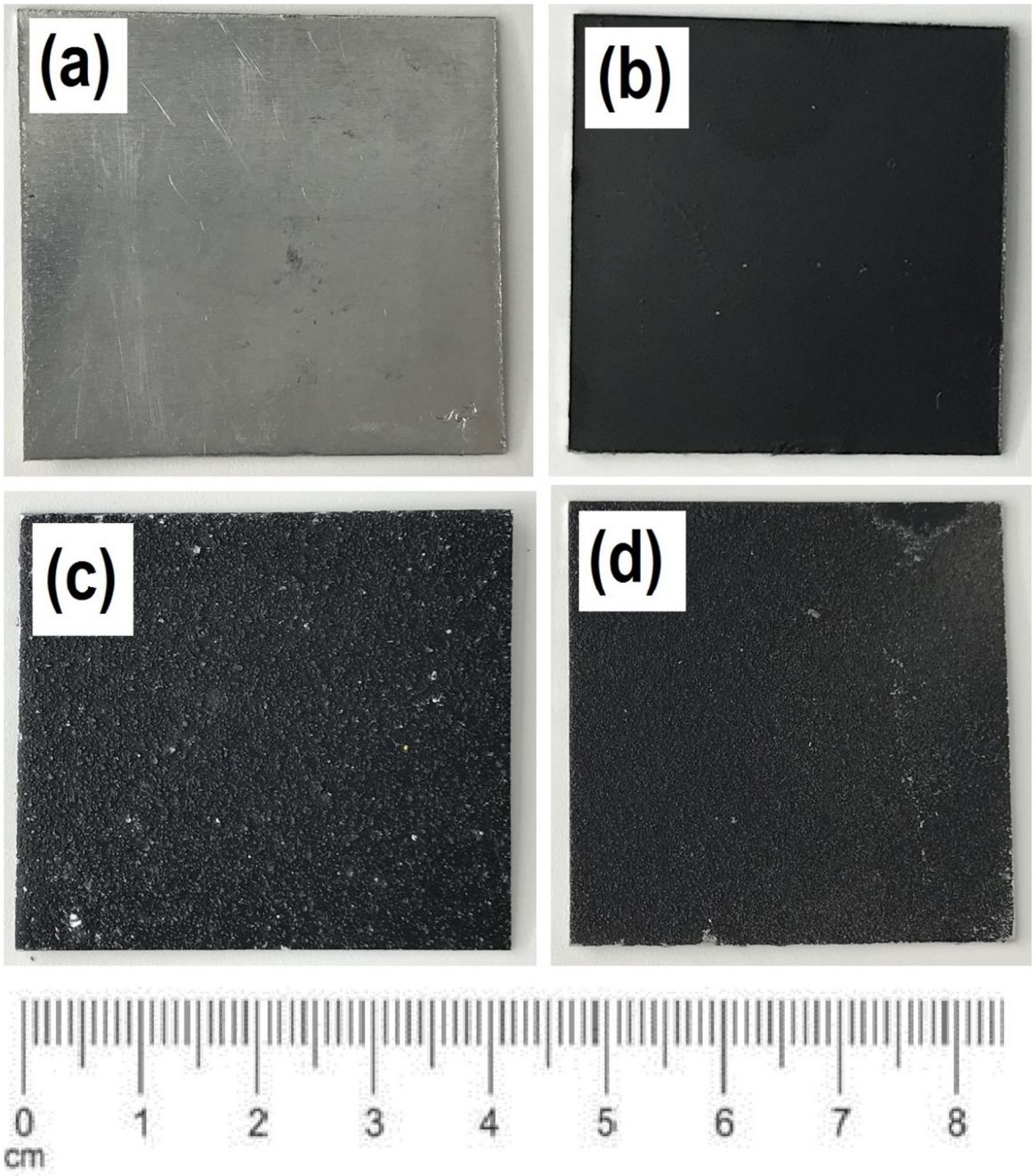

FIG. 1. The aluminum substrates as photographed by an ordinary camera: (a) uncoated substrate, (b) substrate coated with heat-resistant paint (HRP), (c) substrate coated with ZrO_2 powder sprayed over the HRP, and (d) substrate coated with Fe powder sprayed over the HRP.

The coated substrates were also subjected to elemental analysis and mapping via electron energy-dispersive spectroscopy (EDS). This was accomplished using the XFlash-6l10 detector (Bruker Company) attached to the scanning electron microscope. The detector used is advantageous in providing an outstanding resolution of 38 – 121 eV and high pulse load capability. With this detector, low concentrations can be detected with a high degree of relative

precision of 2-4% over a relatively large area (for further details, see Ref. [21]). To compare the coatings and analyze their solar-to-thermal conversion response, UV-Vis spectroscopy was utilized. Comparison of UV-Vis spectra provides valuable insight into the effect of the coating components on their functionality as selective coatings. It also shows the regions where the absorbance of the incident radiation is taking place. By comparing multiple spectra, the degree of radiation absorption at a certain wavelength may further be investigated with the variation of the coating composition (spectral absorbance).

V. Measurements and Test

The solar-to-thermal conversion of the as-prepared coatings was verified by exposing the substrates to radiation and measuring their temperature with time. Each substrate was placed inside a solar collector, as shown in Fig. 2. The solar collector was made of thermally insulating material. The incident radiation passed through the transparent glass window to the substrate. A thermocouple probe attached to a GM1312 digital thermometer (Benetech, Shenzhen Jumaoyuan Science and Technology Co., Ltd., China) was used to measure the substrate temperature. Temperature measurement was performed every 60 seconds, starting from the substrate exposure to radiation until a constant temperature was reached. Two sources of radiation were used in the present work: solar radiation and an artificial source of radiation from a tungsten hot-filament bulb. In the case of an artificial source of radiation, the source-to-collector distance was adjusted such that the total incident irradiance was comparable to that of the solar radiation.

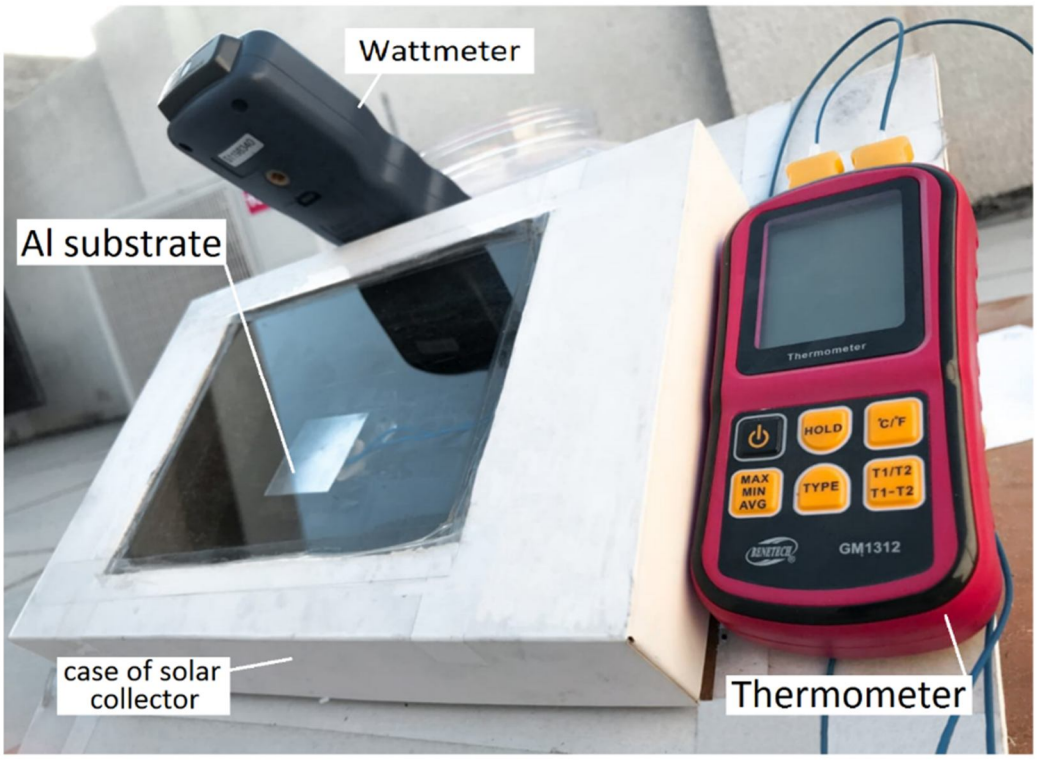

FIG. 2. The solar collector setup used to measure photothermal conversion.

The total reflection of the incident radiation was measured via a homemade pyrheliometer-like setup, as shown in Fig. 3. The device setup allowed measuring the total reflected radiation relative to the incident radiation after excluding the diffused radiation. An SM206-SOLAR digital solar-power meter (Hangzhou Yucheng Industrial Co., Ltd., China) was used to measure irradiance. During the measurement of the total reflectance, the tube was oriented such that the incident radiation formed an angle of 45° with respect to the substrate plane. This guaranteed that most of the reflected radiation was incident perpendicularly on the power meter detector. Comparison of the total reflectance from the substrates can directly be associated with the UV-Vis spectra. The total reflectance is useful in the explanation of the behavior of the solar-to-thermal conversion of the coated substrates.

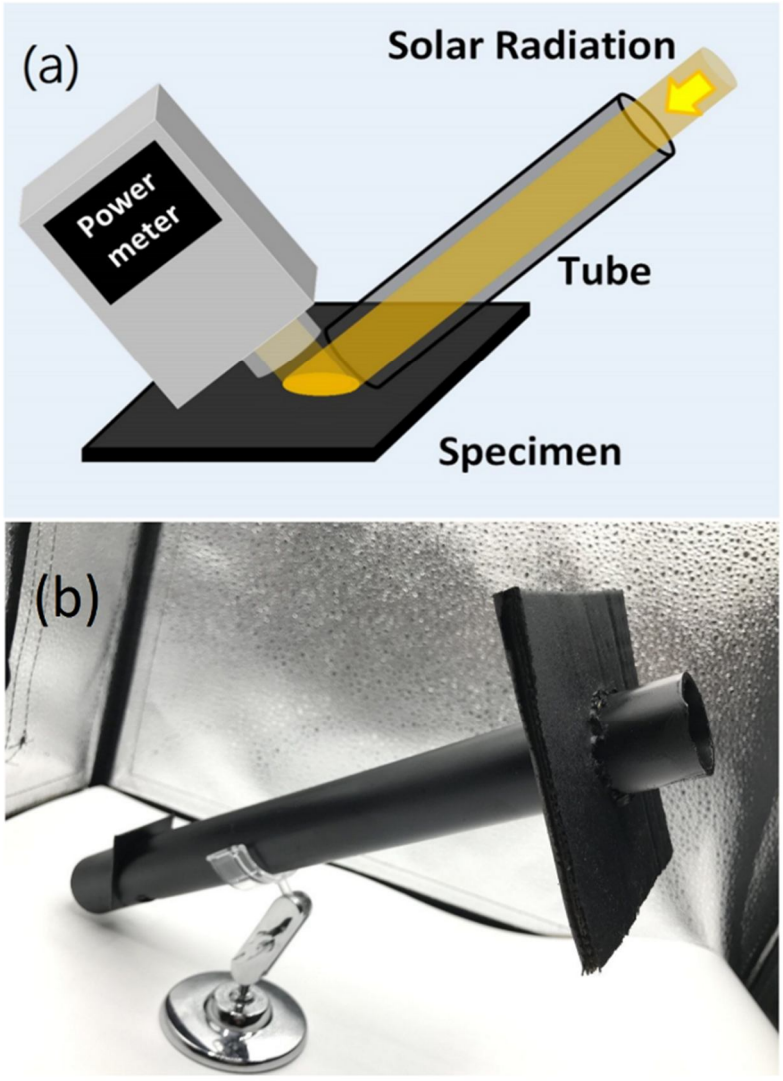

FIG. 3. Homemade pyrheliometer-like setup used to measure the total reflection of incident radiation from the substrate surface: (a) schematic diagram showing the paths of incident and reflected beams of the solar radiation; (b) the experimental setup.

3. Results and Discussion

Figure 4 shows the as-coated substrates under an optical microscope. Primary inspection of the uncoated substrate shows the presence of longitudinal and unidirectional grooves resulting from the brush cleaning performed on the substrate. These grooves became less visible as being filled with the primary coating (the HRP). This ensures the required adhesion of the primary coating on the Al substrate. The addition of the powders on the top of the primary coating is evident in Figs. 4 (c) and 4(d). Comparison of these images shows that the ZrO_2 particles are less homogeneously distributed on the surface of the substrate. The ZrO_2 particles (or their agglomerates) are larger than the Fe particles, as was primarily observed in the photographed substrates (Fig. 1). The distribution feature of the particles is believed to be a direct result of the spraying process adopted in the present work: smaller particles are more easily dispersed uniformly over the substrate surface. Consequently, the Fe particles exhibited better dispersion and more uniform coverage than the ZrO_2 particles.

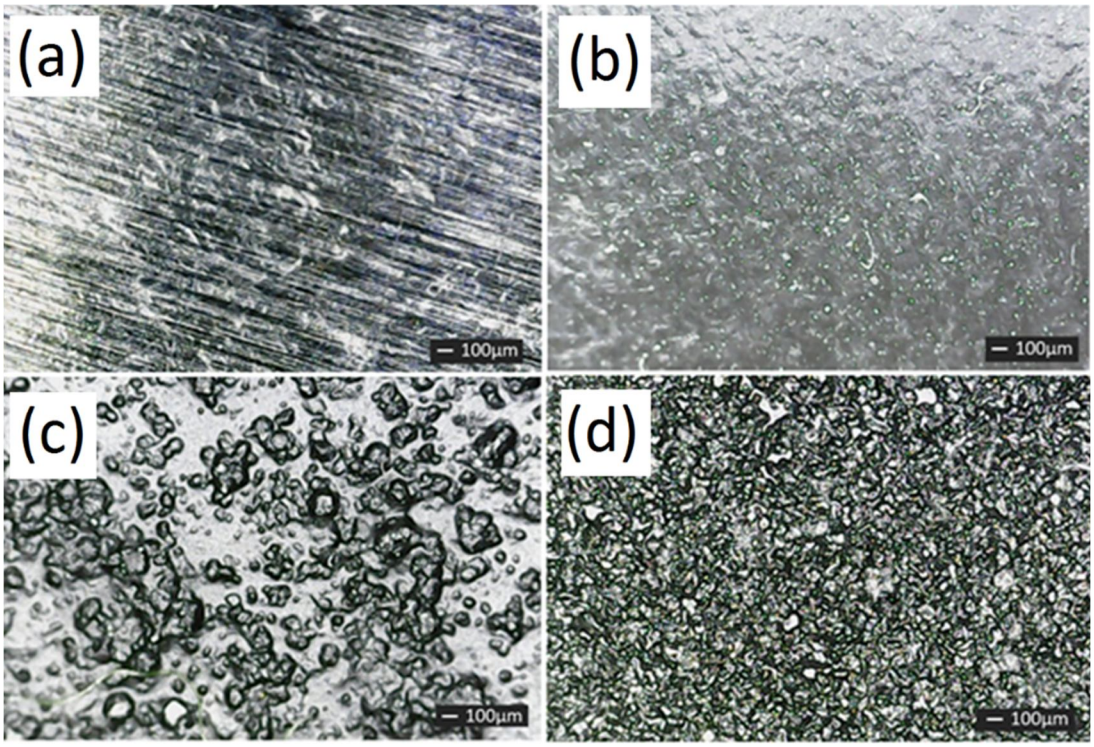

FIG. 4. The substrates under the optical microscope: (a) uncoated, (b) coated with HRP, (c) coated with ZrO_2/HRP, and (d) coated with Fe/HRP.

Table 2 summarizes the average coating thicknesses obtained from multiple measurements, along with the coating masses measured using a coating thickness gauge and a high-accuracy digital balance. The gross density of the coating layer was determined, in addition to its volume and weight. These specifications will be associated with the coatings' photothermal conversion characteristics at the end of this discussion. It is clear that adding ZrO_2 and Fe particles increased the coating thickness and mass and decreased the coating density. This is attributed to the increase in surface roughness due to the partial submerging of particles in the primary coating.

TABLE 2. Coatings thicknesses and densities.

Coating	Coating thickness (μm)	Coatings mass (g)	Coating Density (g/cm^3)
HRP	41	0.11	1.67
ZrO_2/HRP	323.5	0.16	0.31
Fe/HRP	837	0.67	0.50

A further inspection of the coating morphology and particle distribution was performed using scanning electron microscopy. The SEM images of the ZrO_2/HRP and the Fe/HRP are shown in Fig. 5. The former composite coating exhibited agglomeration of the ZrO_2 particles. The high-magnification image showed the presence of sub-micro and nanoparticles diffused in the HRP. The Fe/HRP coating exhibited a denser distribution of the Fe particles, which also showed a high degree of agglomeration. The HRP was highly occupied with the Fe agglomerates, submerged partially in the primary coating. Closer inspection of the powders revealed the presence of boundaries between agglomerated grains, indicating that the actual sizes of these grains were in the sub-micro and nanoscale. These microstructural features were expected to play a significant role in the functional performance of the coatings. The particles were anticipated to act as absorption centers for incident electromagnetic radiation, while the interparticle spaces and voids could serve as radiation-trapping sites. Such effects were expected to enhance solar absorption through scattering and multiple internal reflections [22]. The higher particle density observed in the Fe/HRP coating compared with the ZrO_2/HRP coating was a direct consequence of the coating process, as reflected in the increased thickness and mass of the Fe-containing coating layer (Table 2).

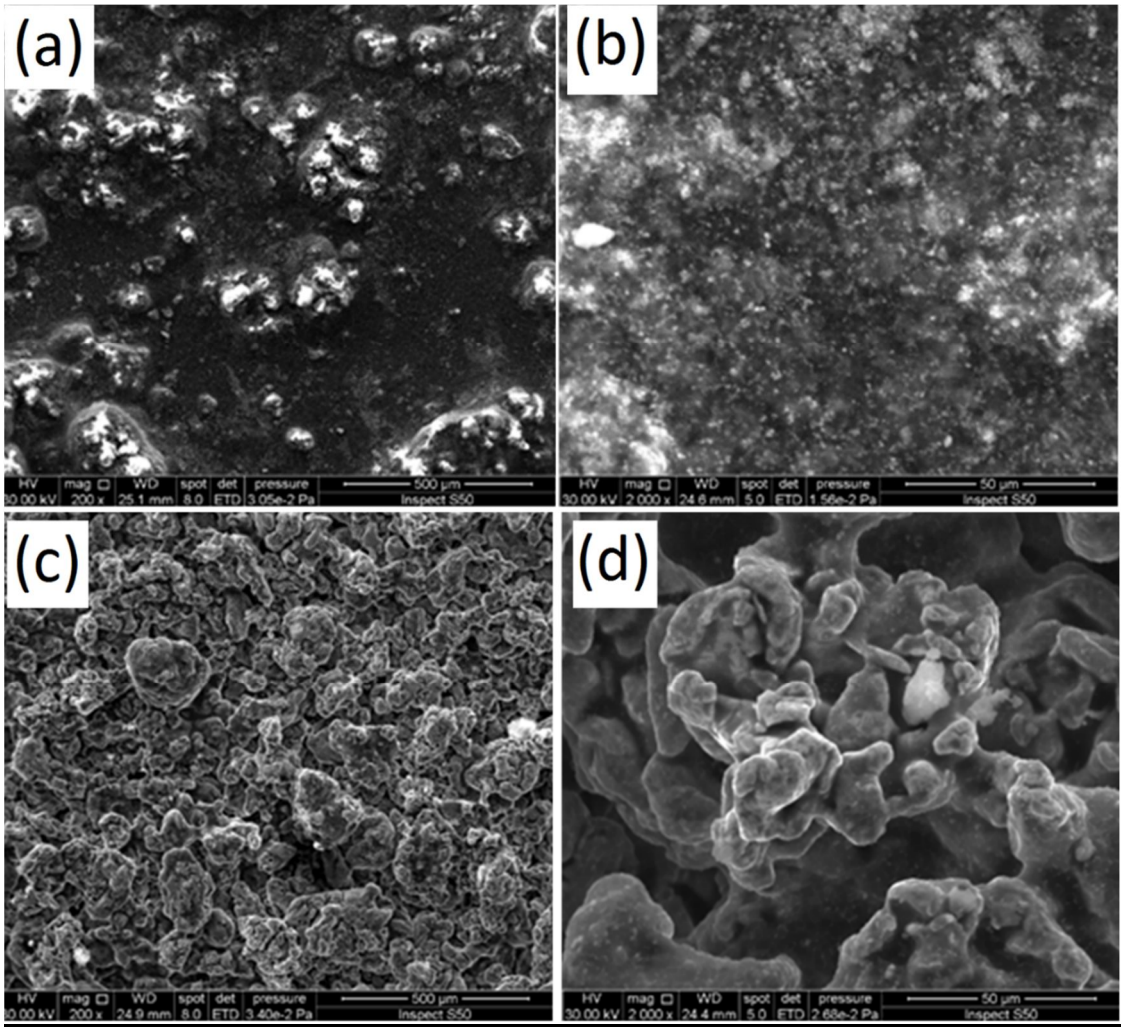

FIG. 5. Low- and high-magnification scanning electron micrographs of the substrates: (a), (b) as coated with the ZrO_2/HRP, and (c), (d) as coated with the Fe/HRP. High-magnification images show that particles are submerged in the HRP.

The elemental analysis results emphasized the distribution nature of these particles. The EDS spectra and the elemental mapping images of the ZrO_2 and Fe particles are shown in Figs. 6 and 7, respectively. The presence of Zr and Fe in their respective substrates can easily be observed. The elemental mapping emphasized that the Fe density distribution was much higher than that of Zr. These results agree with the earlier inspection made under optical and scanning electron microscopes. As for the remaining elements detected (such as carbon and chromium), these are due to the constituting materials of the heat-resistant paint used in the present work and the impurities present at the surface of the substrates.

The photothermal conversion of the as-prepared coatings was examined using the solar and artificial radiation sources. Figure 8 shows the variation of substrate temperature with the duration of exposure to the radiation. The photothermal conversion graphs show that the substrate temperature increased rapidly starting from the room-temperature value with radiation exposure. Initially, the temperature rose rapidly due to radiation conversion into thermal energy and the substrate's low rate of energy loss. After approximately 10 minutes of exposure to radiation, the rate of temperature increase of the substrate decreased, and the solar-to-thermal conversion curve gradually flattened. The substrate temperature reached a maximum and constant value after 35 minutes of radiation exposure. At this point, the rate of solar-to-thermal conversion became equal to the rate at which the substrate lost energy. The uncoated substrate exhibited the lowest temperature due to the low coefficient of absorption of the uncoated surface. The Fe/HRP-coated substrate showed the highest temperature of 382.65 K after 40 minutes of radiation exposure. This was due to

the high coefficient of absorption of the composite coating, which improved the photothermal conversion. In addition, the morphological and surface features (roughness as observed under the scanning electron microscope and reduced density as discussed earlier in this section) are believed to play a crucial role in improving the conversion efficiency via trapping of incident light and its absorption by scattering and multiple reflections (see Ref. [8]). Based on that, future work will attempt to investigate the effect of surface gap density on photothermal conversion efficiency. The quantification of such an effect is believed to provide an effective means to advance selective coatings. As mentioned earlier, the enhancement of the photothermal conversion of ZrO_2/HRP and Fe/HRP may involve different mechanisms. Presently, the results were analyzed by comparing the elemental, compositional, and structural features of the coating in addition to comparing the absorption spectra in the UV-Vis wavelengths, as shown below.

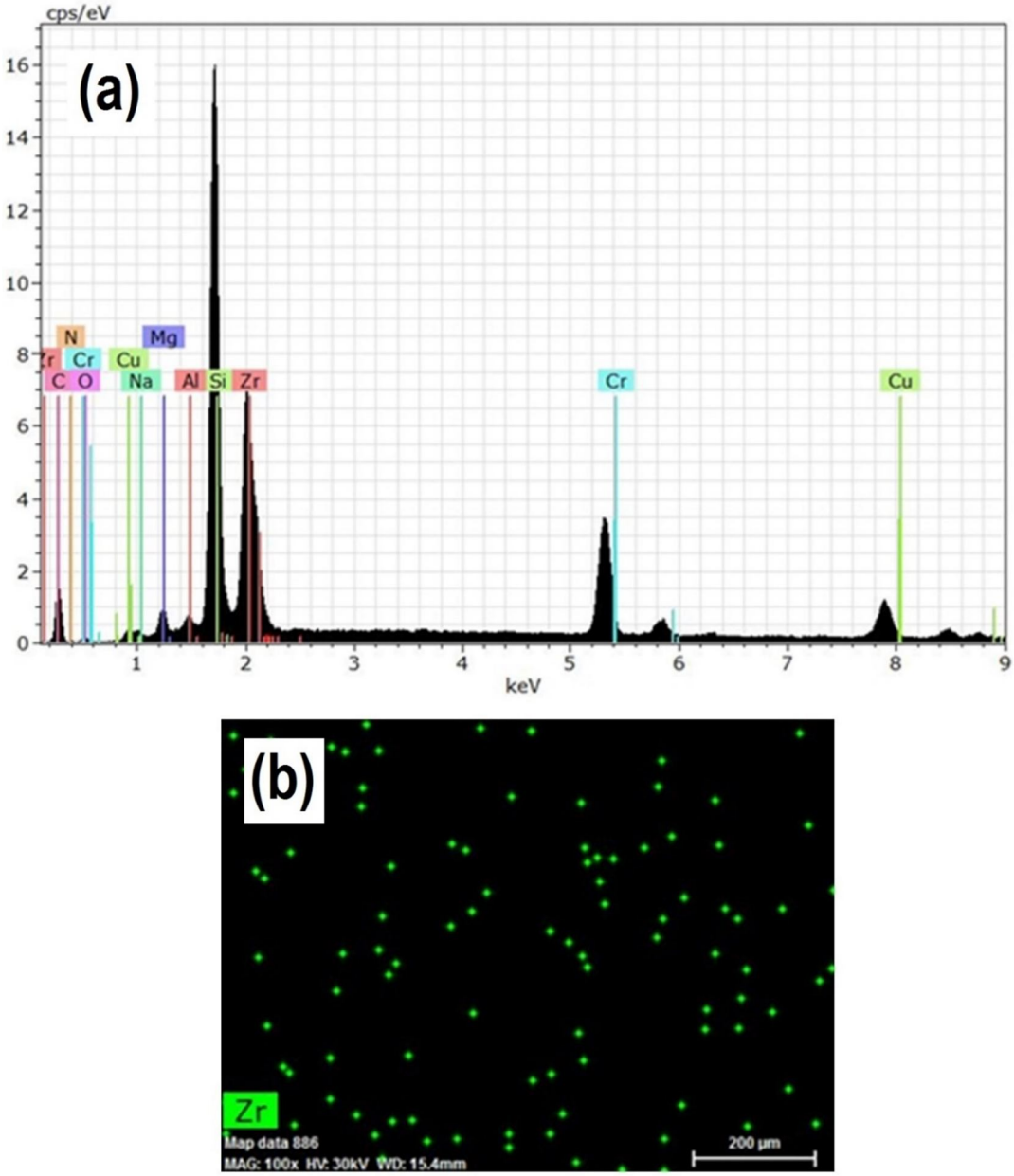

FIG. 6. (a) EDS spectrum and (b) elemental mapping image of the ZrO_2/HRP coating.

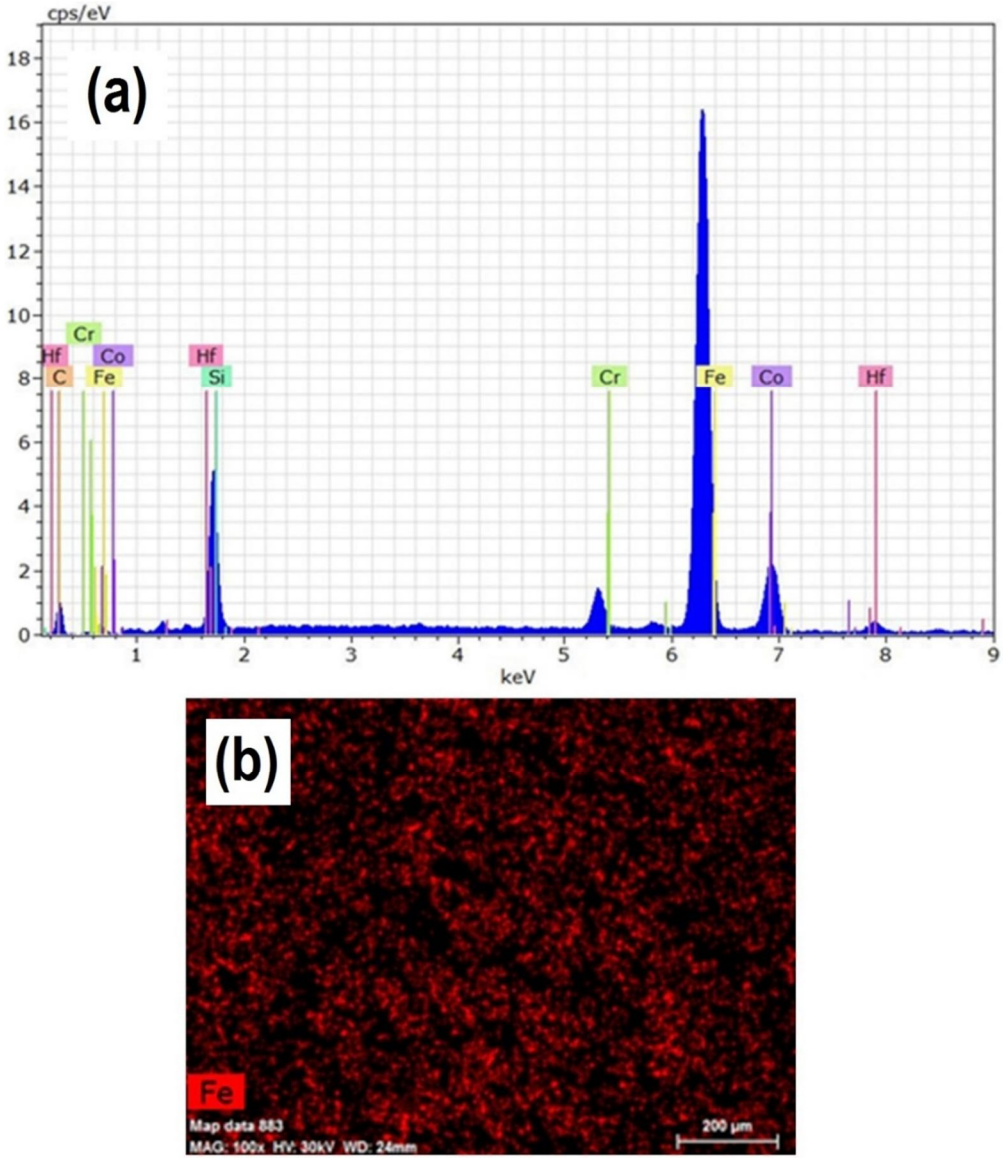

FIG. 7. (a) EDS spectrum and (b) elemental mapping image of the Fe/HRP coating.

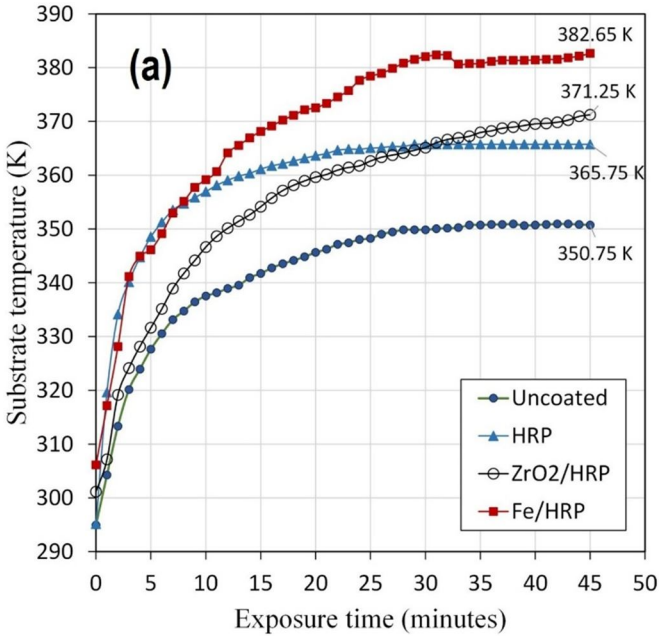

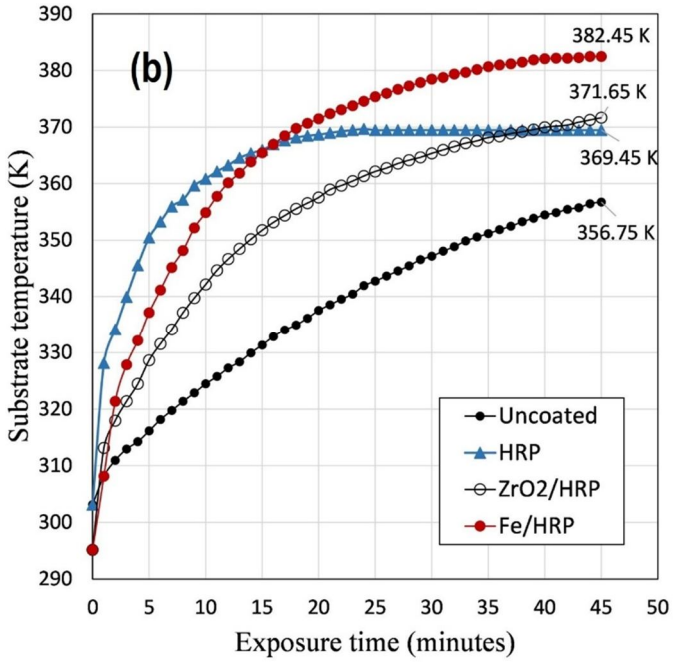

FIG. 8. Photothermal conversion curves of the substrates: (a) exposure to solar radiation and (b) exposure to an artificial source of radiation (hot filament bulb).

As far as we know, the substrate temperature reported presently is the highest for a flat-plate collector setup. Table 3 shows a comparison of the maximum temperature achieved for flat-plate collectors with different composite coatings.

TABLE 3. Comparison of the substrate maximum temperatures for different coatings.

Coating Type	Irradiance (W/m^2)	$T_{substrate}\,(K)$	Reference
Fe/HRP	1130	382.65	Present work
ZrO_2/HRP	1074	371.25	Present work
CNT-CuO NPs dispersed in black paint	964	357.45	[23]
CuO NPs mixed with black paint	1100	370.15	[11]
NiAl alloy embedded in black paint	1000	342.85	[24]

To shed more light on the thermal conversion characteristic of the coatings, UV-Vis spectra were measured for the composite coatings. The absorption spectra of the ZrO_2/HRP and Fe/HRP coatings are shown in Figs. 9(a) and 9(b), respectively. Both spectra showed absorption peaks at 314 nm, 437 nm, 471 nm, and 495 nm. The absorption bands in the wavelength 314 nm might be attributed to the $n \rightarrow \pi^*$ transition due to promoting a non-bonding electron to an anti-bonding π^* orbital [25]. This transition was attributed to the presence of C = O bonds in acetone and xylene in the heat-resistant paint (see Table 1). The absorption peak at 437 nm was attributed to conjugated planar ring structures with delocalized π-electron systems involving alternating single and double bonds, primarily associated with the toluene component of the base paint. The absorption peaks at 471 and 495 nm were attributed to pigments and dyes used in the paint formulation [26, 27]. Accordingly, the ZrO_2/HRP and Fe/HRP composite coatings exhibited identical UV-Vis spectra in the visible wavelengths and differed in the near-infrared regions, signifying the higher contribution of molecular vibrations as compared with the electronic transitions in the overall absorption of radiation. This implies that the mechanism involved in the enhancement of the photo-thermal conversion depends largely on trapping and multiple reflections of radiation near the coating surface due to the morphological complexity produced by the addition of the ZrO2 and Fe particles. Inspection of the SEM images (Fig. 5) supported this interpretation, as the Fe/HRP coating exhibited a higher surface roughness than the ZrO_2/HRP coating.

Comparison of the UV–Vis spectra further showed that the area under the absorption curve, which represents the total absorbed radiation, was larger for the Fe/HRP composite coating. To

validate this observation, the total absorbance of the substrates was determined from total reflectance measurements performed using the pyrheliometer-like setup. Table 4 lists the absorbance values for the four substrates investigated. The calculations showed that the Fe/HRP-coated substrate absorbed 97.81% of the total incident radiation, which was the highest among all coatings studied. This high absorbance was consistent with the elevated substrate temperature of 382.65 K observed during photothermal conversion measurements (Fig. 8).

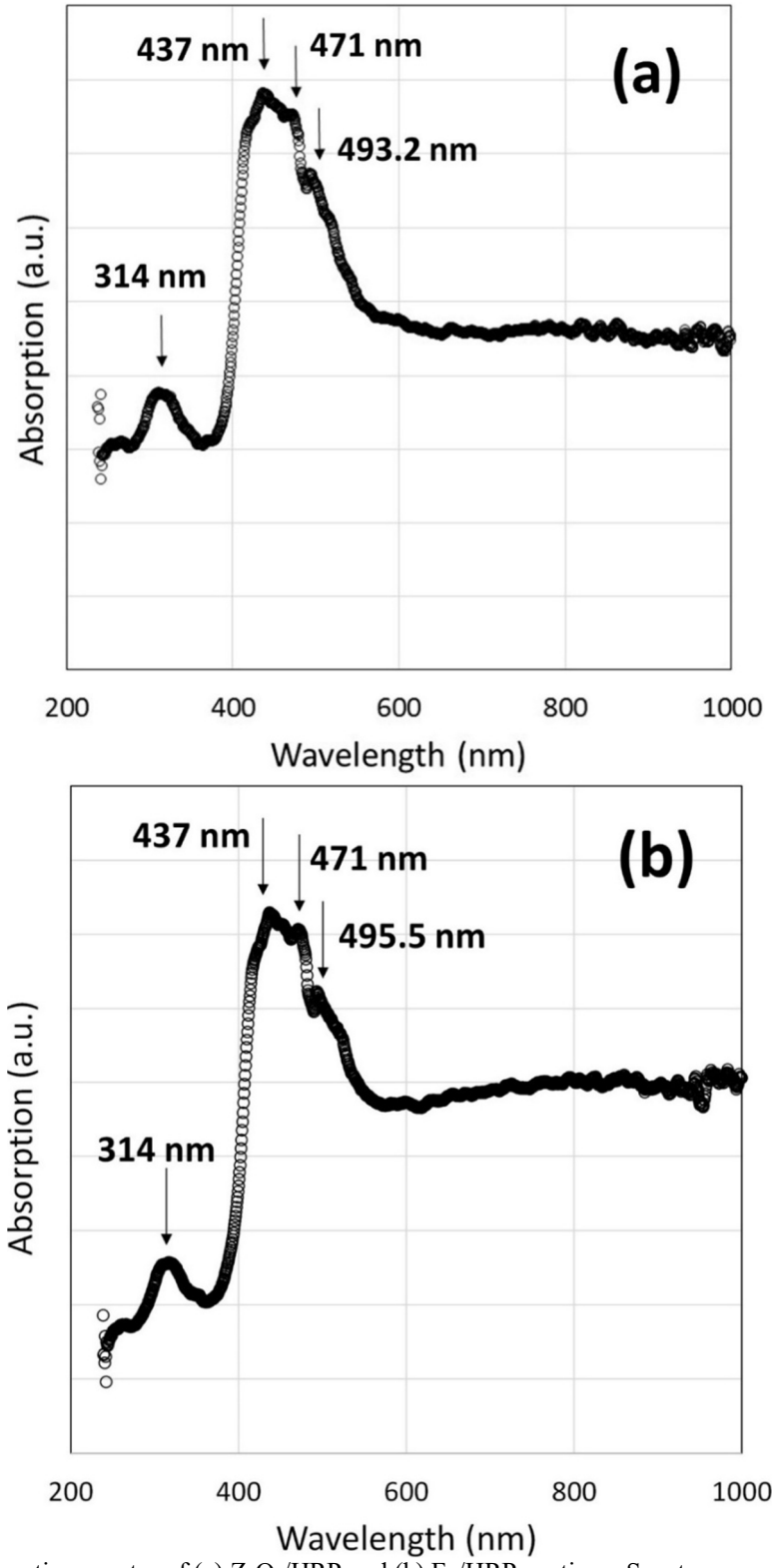

FIG. 9. UV-Vis absorption spectra of (a) ZrO_2/HRP and (b) Fe/HRP coatings. Spectra were determined from the reflection spectra measured experimentally.

TABLE 4. Absorbance of the uncoated and coated substrates, determined using the pyrheliometer-like setup.

Coating	Irradiance (W/m^2)	Total Reflected Intensity (W/m^2)	Absorbance (%)
Uncoated Al-substrate	1186	760	35.91
HRP	1186	67	94.32
ZrO_2/HRP	1188	43	96.38
Fe/HRP	1145	25	97.81

4. Conclusions

In this work, the photothermal conversion characteristics of a selective coating designed for flat-plate collector applications were investigated. ZrO_2 and Fe particles were incorporated into a heat-resistant paint (HRP) to enhance its solar-to-thermal conversion performance. The coating thicknesses were 323.5 and 837 μm for the ZrO_2/HRP and Fe/HRP coatings, respectively. The addition of ZrO_2 and Fe particles led to a decrease in coating density from 1.67 g/cm^3 to 0.31 and 0.5 g/cm^3 for the ZrO_2//HRP and Fe/HRP coatings, respectively. The solar-to-thermal conversion of the coatings was successfully improved due to the addition of these particles. A maximum absorbance of 97.81% of the incident radiation was achieved using the Fe/HRP composite coating. The maximum substrate temperature of the flat-plate collector setup was 382.65 K after 40 minutes of exposure to solar radiation. The high photothermal conversion characteristics and the ease of preparation and application of the Fe/HRP coating make it superior to other coating systems with varying structural, compositional, and morphological properties.

Declaration of interests

The authors declare that they have no known competing financial interests or personal relationships that could have appeared to influence the work reported in this paper.

Data availability

Data will be made available on request.

References

[1] Omer, K.A., Sameer, A., Raid, W.D., Hawazen, N.S., and Enas, F.A., Int. J. Renew. Ene. Dev., 12 (1) (2022) 166.

[2] Noc, L., Jerman, I., Sol. Energy Mater. Sol. Cells, 238 (2022) 111625.

[3] Gao, M., Zhu, L., Peh, C.K., and Ho, G.W., Energy Environ. Sci., 12 (2019) 841.

[4] Bhowmik, H. and Amin, R., Energy Rep., 3 (2017) 119.

[5] Vikas, Kumar, R., and Soni, S., Beilstein J. Nanotechnol., 14 (2023) 205.

[6] El-Mahallawy, N., Atia, M.R.A., Khaled, A., and Shoeib, M., Mater. Res. Express, 5 (2018) 046402.

[7] Wasim, M., M.Sc., Thesis, University of Eastern Finland, Faculty of Science and Forestry, (2024).

[8] Cheng, P., Wang, D., and Schaaf, P., Adv. Sust. Syst., 6 (2022) 2200115.

[9] Rubin, E.B., Chen, Y., and Chen, R., Solar Energy Mater. Sol. Cells, 195 (2019) 81.

[10] Atchuta, S.R., Sakthivel, S., and Barshilia, H.C., Sol. Energy Mater. Sol. Cells, 200 (2019) 109917.

[11] Sivakumar, S., Velmurugan, C., Ebenezer Jacob Dhas, D.S., Brusly Solomon, A., and Leo Dev Wins, K., Renew. Energy, 155 (2020) 1165e1172.

[12] Zerouali, M., Bouras, D., Daïra, R., Fellah, M., Boudjema, B., Barille, R., Sakherf, E., Bellucci, S., and El-Hiti, G.A., Ceram. Int., 51 (2025) 473.

[13] Bouras, D., Fellah, M., Barille, R., Zerouali, M., Hambli, N., and El-Hiti, G.A., Inorg. Chem. Commun., 171 (2025) 113561.

[14] Sadia, A., Ifra, S., Farzana, M., Ismat, B., Ijaz-ul-Mohsin, Kashif, J., Yassine, S., and Munawar, I., Z. Phys. Chem., 2020 (2020) 1.

[15] Elangbam, C.D. and Ibetombi, S., Adv. Mater. Process., 2 (2) (2017) 93.

[16] Jasim, R.H. and Al-Tabbakh, A.A., Jordan J. Phys., 15 (3) (2022) 323.

[17] Jasim, R.H., Al-Tabbakh, A.A., and Hasan, S.M., Al-Nahrain J. Sci., 24 (1) (2021) 24.

[18] Kohli, R., Develop. Surf. Cont. Clean., 2015 (2015) 71.

[19] Petersson, L., Meier, P., Kornmann, X., and Hillborg, H., J. Phys.: Appl. Phys., 44 (3) (2011) 34011.

[20] Kadlečková, M., Minařík, A., Smolka, P., Mráček, A., Wrzecionko, E., Novák, L., Musilová, L., and Gajdošík, R., Mater. (Basel), 12 (1) (2018) 109.

[21] https://www.bruker.com/en/landingpages/bna/technology/what-is-eds.html.

[22] Xie, Z., Wang, H., Li, M., Tian, Y., Deng, Q., Chen, R., Zhu, X., and Liao, Q., Chem. Eng. J., 435 (3) (2022) 135025.

[23] Abdelkader, T.K., Zhang, Y., Gaballah, E.S., Wang, S., Wan, Q., and Fan, Q., J. Clean. Prod., 2019 (2019) 119501.

[24] Al-Shamaileh, E., Sol. Energy, 84 (9) (2010) 1637.

[25] https://chem.libretexts.org.

[26] Tomovska, R., Agirre, A., Veloso, A., and Leiza, J.R., "Reference Module in Chemistry, Molecular Sciences and Chemical Engineering", (Elsevier, 2014).

[27] Masahiko, T. and Jonathan S.L., Digit. Discov., 4 (2025) 21.